Effect of H-ZSM-5 acidity in methanol-to-olefins conversion

Beatriz Estevens C. B.[1], Marie-Elisabeth Lissens[2], Pedro S. F. Mendes[1,2], Maria Filipa Ribeiro[1], Joris Thybaut[2]

[1] Chemical Engineering Department, Instituto Superior Técnico, Lisbon, Portugal

[2] Laboratory for Chemical Technology, Ghent University, Ghent, Belgium

October 2021

Abstract

From environmental awareness to the energetic transition, nowadays society faces one of its biggest challenges in order to prosper in a sustainable path. Methanol-to-olefins process arises with the promise of a circular economy and carbon neutrality in the battle against fossil fuels in the propylene market. With increasing projects on green methanol pathways, it is essential to study and optimize this industrial technology in terms of reaction conditions, kinetics, and catalyst design to maximize propylene yielding. The present work studied the effect of acidity in commercial H-ZSM-5 catalysts (Si/Al of 25, 40 and 140) in the reaction pathways of MTO within the dual-cycle mechanism concept. Elemental, textural, and acidic properties were investigated. Catalytic studies were carried out at constant 0.4 bar methanol partial pressure, steady-state, and under intrinsic kinetic regimes, between 350-450º C on an isothermal tubular reactor. Increasing temperature favoured higher propylene yields by promotion of the alkene cycle up to 375º C. At higher temperatures, the effect of acidity was manifested through the increasing promotion of the aromatic cycle due to the decrease in $Brønsted_{strong}/Lewis_{total}$ acid sites ratio. A maximum of contribution of the aromatic cycle was determined to occur in a catalyst with a Si/Al ratio between 40 and 140. Lewis acid sites were linked to the stabilization of poly-aromatic intermediate species and to higher apparent activation energies, which established MTO as a two-site reaction mechanism kinetics. Catalysts with lower acid site density, higher relative mesopore volume, and higher external surface area presented lower deactivation rates and improved propylene yields. H-ZSM-5 with Si/Al of 140 displayed the best performance with a good propylene maximization and a high catalytic lifetime. Future studies on the effect of acidity should aim to validate these results through more studies (H-ZSM-5 with Si/Al ratios above 100).

Keywords: methanol-to-olefins; MTO; intrinsic kinetics; steady-state; H-ZSM-5; acidity; Brønsted; Lewis.

1. Introduction

The growing environmental awareness led the European Commission to set a target goal of 60% reduction of carbon dioxide emissions by the end of 2030 and carbon neutrality by 2050 [1-3]. Carbon-intensive industries, such as the cement and iron industries, are presented with the great opportunity of turning their waste into a resource [2]. The energy and chemicals sectors face the great challenge of satisfying the market demand and finding environmentally sustainable alternatives to fossil fuels. Therefore, there is a pressing necessity to make a swift and targeted change in all industries for a circular economy.

Polyolefins are the major building blocks of polyethylene and polypropylene [4]. The increasing demand for propylene has directed the search for selective and environmentally conscious technologies in recent years [5-8]. Methanol-to-olefins (MTO) appears as an emergent technology. Methanol is produced from synthesis gas (a mixture of carbon monoxide and hydrogen,) which can be most commonly obtained from steam reforming of natural gas and coal gasification [9-11]. Methanol production is presented as a great opportunity towards carbon neutrality by the use of the carbon footprint of other industries in this process. In Belgium, the North-C-Methanol plant, with a methanol production capacity of 44 ktpa, is a landmark for these principles by also incorporating hydrogen production from renewable energy [12].

MTO has been under study since the early '70s over SAPO-34 and H-ZSM-5 zeolites. Over 20 mechanisms have been proposed to describe the formation of the first C-C bond [13, 14]. Although it remains an unanswered question, this step has been considered to be of little practical importance for the understanding of the mechanistic pathways at steady-state [15]. MTO reaction exhibits an autocatalytic behaviour catalysed by the zeolite's acidic sites, starting with a slow methanol conversion rate at low space-times, noted as the induction period with the formation of a pool of aromatic species [15]. This period is followed by an increase in the rate of conversion with the progression of olefin production [16].

The dual-cycle mechanism (Figure 1), proposed by Svelle et al. (2006) is currently the most widely accepted mechanism for MTO at steady-state [17]. It is a refinement of the initial hydrocarbon pool mechanism (HCP)proposed by Dahl and Kolboe in 1994 [18]. The work of Svelle. et al. advocates that HCP species are formed during the initial stage of the reaction where methanol follows a succession of condensation, alkylation, cyclization, and hydrogen transfer reactions [15].

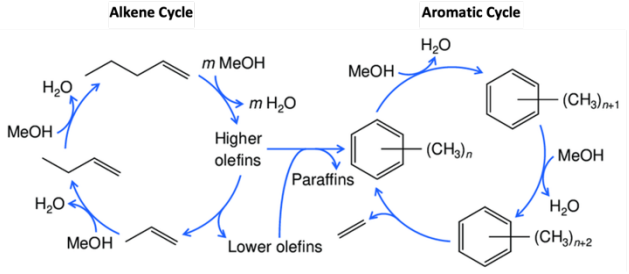

Figure 1 – Representation of MTO dual-cycle mechanism over H-ZSM-5. Adapted from [62].

The poly-methylbenzene (polyMB) species formed undergo aromatic methylation and dealkylation reactions, eliminating ethylene and propylene, which resumes the aromatic cycle [19]. Aromatics are being constantly produced through the aromatization of higher alkenes [15]. These olefins are formed through the propagation alkene cycle by a series of methylation, oligomerization, and cracking reactions [15]. The increase in temperature has been linked to the propagation of the alkene homologation cycle (by which C_3-C_7 olefins are formed), while catalyst acidity has been reported with scattered results with little consensus between authors [20-26].

However, there is a blatant disregard for ensuring that data is acquired at steady-state and under no influence of transport phenomena. Afterwards, data undergoes a deactivation assessment study. The present work performs a comprehensive study on the effect of acidity on the mechanistic pathways of MTO, within the dual-cycle concept. Catalytic studies are performed at constant methanol partial pressure, acquired at steady-state and intrinsic kinetic regime, over commercial H-ZSM-5 zeolites with Si/Al ratios of 25, 40 and 140.

2. *Experimental Procedures*

2.1. Catalyst Preparation The commercial ZSM-5 zeolites were acquired in their ammonium form from Zeolyst with Si/Al ratios of 25, 40 and 140 (CBV 5524G, CBV 8014, CBV 28014, respectively). These samples were calcinated to produce their acidic form (H-ZSM-5) with dry flowing air at 550º C for 4h (heating rate of 5º C/min). The acidic samples were named S25, S40 and S140, according to their Si/Al ratio.

2.2. Catalyst Characterization Inductively coupled plasma spectroscopy (ICP), powder X-ray diffraction (XRD), nitrogen adsorption-desorption (N_2 physisorption), and pyridine FTIR spectroscopy (py-FTIR) techniques were used to determine the elemental composition, textural, and acidic properties of the samples.

ICP was carried out in IRIS Intrepid II XSP (an equipment from Thermo Scientific) by an outsourced laboratory in the scope of Pessanha (2019) work [27].

XRD was executed in an outsourced laboratory with a Bruker D8 Advance equipment, motorized by a anti-scatter screen and Autochanger, using a LynxEye XE-T Silicon strip line detector and a CuKα radiation source (Bragg-Brentano geometry), thru a 2θ range of 0.5° to 90°.

N_2 physisorption (77 K) was performed in the Micrometrics Tristar II apparatus between 0.01-1.00 p/pº. All samples were degasified for 8 h at 200º C prior to this analysis.

Py-FTIR was also executed in an outsourced laboratory. The experimental procedure consisted of outgassing the sample (~20 mg) under vacuum (pressure lower than 10^{-5} Pa) at 450 °C for 2h. The sample's IR spectrum was then acquired by subtracting the background spectrum of the empty cell. After releasing the vacuum, the sample was cooled down and stabilized at 150º C where a background spectrum was recorded. It followed successive releases of small portions of pyridine, intercalated with outgassing of physiosorbed species. The procedure was repeated until no further changes in the peak intensities were observed in the differential spectra. Differential spectra were acquired for 150º, 250º, 350º and 450º C for each catalyst sample. Data at 350º and 450º C was not possible to acquire for S140. Considering the results from the previous techniques and the work of Busca et al. (2014), since Lewis acidity was retained throughout the studied desorption temperatures, studies followed the consideration that twice of Brønsted acidity was best preserved for S140 comparing to S25 [28].

2.3. Catalytic Studies Catalytic studies were executed at Laboratory for Chemical Technology (LCT, Ghent University), in the HTK (high throughput kinetic) setup designed by Zeton B.V. for intrinsic kinetic data acquisition.

The catalytic reactions were carried out in a stainless-steel isothermal tubular reactor (780 x 11 mm as "length x diameter"), equipped with a 3 mm internal thermocouple. Catalyst loadings varied according to the foreseen experimental conditions (temperature, W/F intervals) and H-ZSM-5 zeolite acidity. Catalyst beds were prepared with palletizing and sieving of the catalysts' samples for particle sizes within the 20-250 μm and diluted with α-aluminum to ensure intrinsic kinetics regime (simulated by EUROKIN online software). In order to avoid particle dragging, a thin bed of glass wool was placed at the bottom of the catalyst bed inside the reactor. System pressure was maintained constant throughout all experiments, with a total pressure of 3.5 bar and methanol partial pressure of 0.4 bar, where nitrogen was used as the dilutant gas in the gas feed. Experiments were conducted between 350º and 450º C, with space-times (W/F) ranging from 0.5 to 40.0 $kg_{cat}.s/mol_{MeOH}$ to achieve the desired conversions.

3. *Results and Discussion*

3.1. Catalyst Characterization

The characterization results from ICP and XRD were as expected for these materials according to the manufacturer's specifications. The XRD results demonstrated that samples evidence a crystalline structure without the presence of impurities. The two-characteristic high-intensity diffraction peaks located at 2θ = 5-10º and the five peaks located at 2θ = 23-25º corroborated the preservation of the MFI structure after calcination [29]. Using the peak at 2θ = 23 as a reference value, the higher intensity of the diffraction peaks at lower angles in S140 reflected the higher silicon content of the zeolite [30].

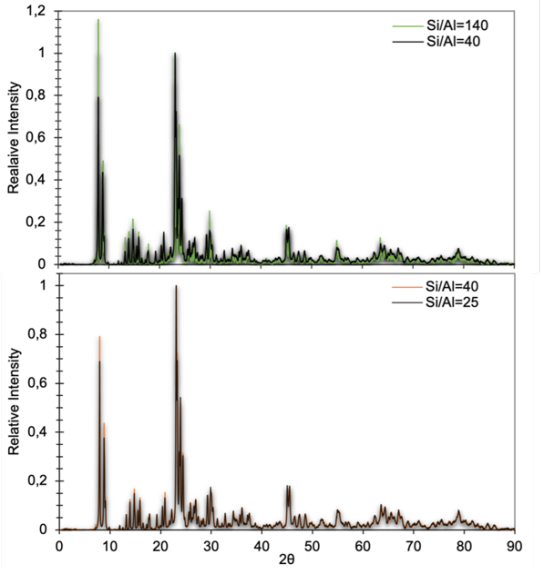

Figure 2 – Comparison of H-ZSM-5 XRD patterns obtained for (top) S140 and S40, and (bottom) S25 and S40.

This effect was most noticeable when comparing S140 to S40 (Figure 2) as predicted by the Si/Al differences. Overall, the good resolution of the patterns confirmed the high crystallinity of the acidic forms of the zeolite samples.

N_2 physisorption concluded that the calcination process preserved the zeolite's framework whilst also promoting microporosity for S140. Furthermore, all calcinated samples displayed similar pore volume and average pore diameter (table 1). However, S140 verified a tangible lower percentage of mesopore volume and higher external surface area, evidencing the higher mesoporosity of the catalyst [31, 32].

Furthermore, the type I and type IV (with hysteresis loop type H4) substantiated the presence of microporous and mesoporous materials [31]. These results were substantiated by previous reports for H-ZSM-5 with these Si/Al ratios [22, 32-34].

The structural defects identified in the IR spectra of the S25 and S140 (Figure 3), from the band between 3660–3690 cm^{-1} (attributed to extra-framework aluminium species, Al_{EF}), the two bands at 3730-3750 cm^{-1} (internal and external silanol groups), and 3630-3650 cm-1 (silanol nests) evidence the accentuated presence of structural defects in these two catalysts comparing to S40 [35-38]. Interestingly, other studies have reported non-detectable amounts of Al_{EF} species for H-ZSM-5 with Si/Al ratios above 75, which was not the case with the present samples [26, 39, 40]. Nonetheless, it has been reported that zeolites with Si/Al ratios lower than 40 typically presents increasing amounts of Al_{EF} species and other defective sites [26, 39-41].

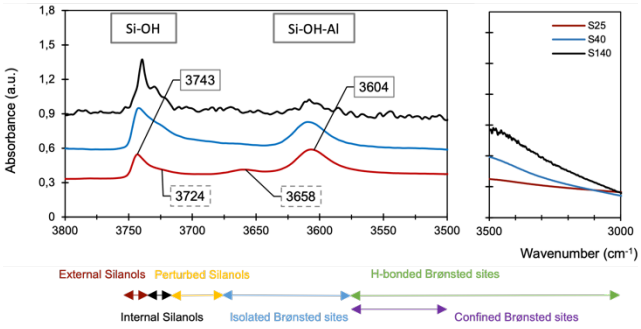

Figure 3 – Normalized IR background spectra for S25, S40 and S140, recorded at 450º C with functional group attribution (adapted from [42]).

The acidic active sites were also investigated FTIR spectroscopy with pyridine as the molecular probe. The vibration bands at 1545 and 1454 cm^{-1} in the differential spectrum were assigned to the adsorption on Brønsted and Lewis acid sites (BAS and LAS), respectively [43-45]. For the quantification of the acid sites, Emeis et al. (1993) molar extinction coefficients were used (2.22 cm/μmol and 1.67 cm/μmol for LAS and BAS, respectively) [46]. The results are presented in Table 1 and depicted in Figure 4.

As expected, an increase in acid site density was confirmed with decreasing Si/Al ratios. At 150º C, S25 presented the highest total acid site density (269 μmol/g), followed by S40 (238 μmol/g) and S140 (63 μmol/g). S140 presented a decrease in almost 80% of acid site density (for

Table 1 – Textural (N_2 physisorption) and acidic properties (py-FTIR) of the calcinated catalysts samples S25, S40, and S140.

Sample	V_{total} (cm^3/g)	V_{micro} (%)	S_{BET} (m^2/g)	S_{micro} (%)	$S_{external}$ (m^2/g)	$D_{pore-average}$ (Å)	n_{LAS} (150/450º C) (μmol/g)	n_{BAS} (150/450º C) (μmol/g)	BAS/LAS (150/450º C)
S25	0.21	48	349	41	143	24	31/25	238/63	7.6/2.5
S40	0.24	47	397	42	168	24	23/26	214/22	9.1/0.9
S140	0.21	32	371	62	230	23	6/6	57/30	9.6/5.0

The micropore volume, micropore area and external area were determined using the t-plot method, whereas the surface area was determined by the BET method. Both the concentration and ratios of acid sites are expressed for 150º and 450º C pyridine desorption temperatures (150/450º C).

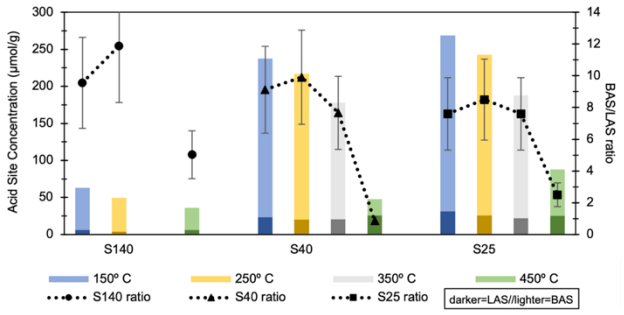

Figure 4 – Total acid site concentrations (bars, with BAS and LAS referred to with lighter and darker colour) and BAS/LAS ratio (points with 15% error bar) results from py-FTIR experiments.

both BAS and LAS) in comparison to S25m which was expected since 80% also corresponds to the variation in aluminium between the two catalysts. Furthermore, these results were very similar to what has been previously reported for H-ZSM-5 with these Si/Al ratios [14, 47].

Still, regarding total acidity, all three zeolites present comparable BAS/LAS ratios, and Lewis acidity was observed to remain preserved throughout experiments. Conversely, S40 presented the lowest BAS/LAS ratios in strong acidity (pyridine desorption at 450º C). Therefore, strong BAS/LAS was demonstrated to be most influenced by BAS. In the case of S25 and S140, it was concluded that strong BAS were stabilized from structural defects (such as internal silanols) as other works had already established [38, 48].

3.2. Catalytic Studies

3.2.1. Deactivation Assessment

The effect of deactivation and transport phenomena hinders the interpretation of product distribution and the mechanistic phenomena occurring behind the effect of operating conditions and catalyst acidity. Consequently, not only catalytic studies were performed under intrinsic kinetic regime at steady-state, but a methodology was also developed to identify data acquired under the effect of deactivation. The severity of deactivation can be associated with known trends, such as higher acid density and lower mesoporosity (together with lower surface areas) from other reports [49, 50]. The created procedure aimed to maximize the amount of information possible to extract from the catalytic experiments. It assesses all data by three assessment stages: first analysing the TOS profile of data, followed by the investigation of catalytic activity and selectivity. The

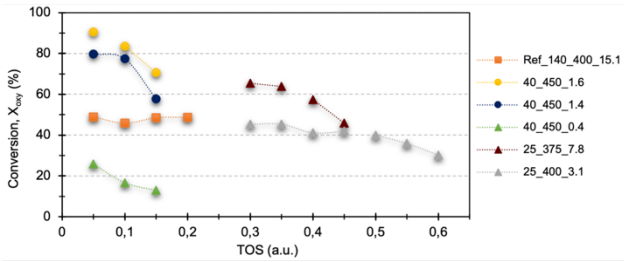

Figure 5 – Oxygenate conversion (X_{oxy}) over S25, S40, and S140, as functions of TOS (a.u.) from consecutive analysis of each dataset at different temperatures and space-times. Legend interpretation: "Si/Al ratio"_"Temperature (º C)"_"space-time ($kg_{cat}.s/mol_{MeOH}$).

investigation relies on contextualizing the data within the dataset where it is inserted, and then linking all information together for the same catalysts and then comparing results.

Data points depcited in Figure 5 identify the effect of deactivation, in S25 and S40, by the decrease of oxygenate conversion between the first and last consecutive analysis (TOS), where steady-state conversion should already be observed. The behaviour of the orange data set (acquired with the S140) illustrates the typical profile expected in the absence of deactivation. On average, S25 presented 4-5h TOS before severe deactivation between 350º-400º C. Within the same temperature intervals, S40 presented the double of catalyst lifetime. The high deactivation rates of these catalysts challenged the catalytic studies and the acquisition of reliable data, compared to S140 which presented over 20h TOS of lifetime at 375º C.

To preserve the information from these experiments (due to the scarcity of available data), the first analysis point was considered to be the closest value to a non-deactivated reference. Figure 6 exemplifies how this analysis is inaccurate by itself. The next stage of the deactivation assessment follows with the evaluation of the catalytic activity of S25 at 400º C represented in grey in Figure 5. Although the first 4 consecutive analyses indicated steady-state conversions, the effect of deactivation by the comparison of activity with data acquired at different space-times is evident in Figure 6.

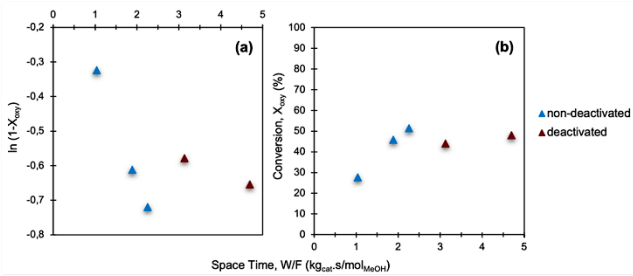

Figure 6 – Plots of (a) ln(1-Xoxy) and (b) conversion of oxygenates (X_{oxy}) over S25 as functions of space-time (T=400º C, P_{MeOH}=0.4 bar, W/F=[1, 5] $kg_{cat}.s/mol_{MeOH}$).

When investigating small data sets, this analysis was determined to be of particular relevance. Furthermore, it was determined that catalytic activity varies between catalyst calcination batches and, therefore, kinetic parameters should be analysed from data originating from the same batch. Nevertheless, it was found that product distribution is not affected in these cases, as depicted in Figure 7.

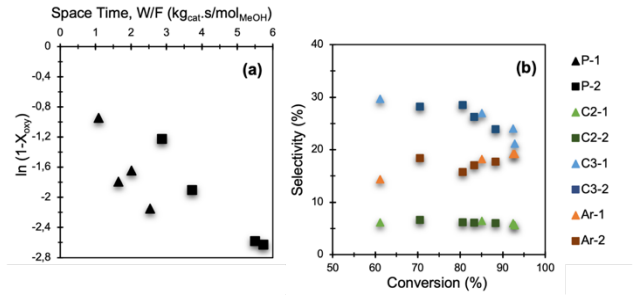

Figure 7 – (a) Catalytic activity plot (with ln(1-X_{oxy}) as function of space time) and (b) selectivity plot as function of conversion (▲: set 1, ■: set 2, colours: different data points) for S40 at 400º C (P_{MeOH}=0.4 bar, W/F=[1, 6] $kg_{cat}.s/mol_{MeOH}$).

Product distribution further demonstrated to retain viable information despite being identified as under the effect

of deactivation (Figure 8). The data points acquired a 10% oxygenate conversion are representative of the effect of conversion at low conversion. As revised, during the induction the aromatic hydrocarbon poll is still being developed and reacts very slowly with the feed, evidencing higher aromatic selectivity and irreproducible results as it is the latter case. Therefore, the best conversion interval at which this reaction was studied hereon was between 20-80%, where the hydrocarbon pool is already fully developed and steady-state regime predominates. Studying MTO at higher conversions brings added challenges for data acquisition without the effect of deactivation and without reaching near-full conversion, where secondary reactions predominate.

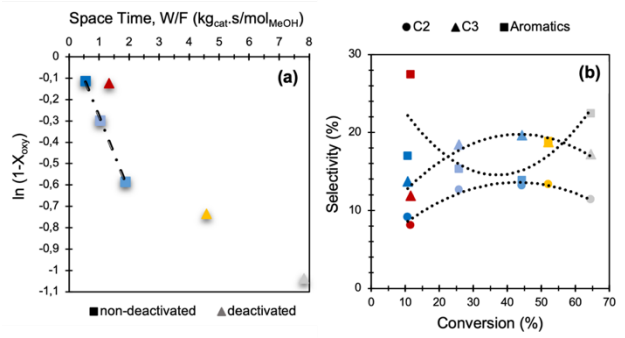

Figure 8 – a) Catalytic activity plot with ln(1-X_{oxy}) as function of space time and (b) selectivity plot as function of conversion (most generally observed trends within 20-80% conversion), for S25 at 375° C (P_{MeOH}=0.4 bar, W/F=[0.5, 8.0] $kg_{cat}.s/mol_{MeOH}$).

Based on this assessment methodology, severe deactivation was noticeable in product distribution by the increase in aromatic selectivity, which was not always accompanied by an increase in ethylene selectivity. As previously explored by several works, deactivation appears to occur due to coke deposition from diffusion resistance and pore-blocking [60]. This phenomenon is most certainly caused by the bulky polyMB species, which are the precursors of the aromatic cycle, thus, the increase in aromatic content. Nonetheless, selectivity is not alone an indicator of deactivation as demonstrated, and all three markers should be taken into consideration: conversion profile, catalytic activity and selectivity, by comparing data within the same data set and with other conditions.

3.2.2 Effect of Catalyst Acidity

Catalytic Activity The study of the effect of acidity resides as the central part of the present work. For that purpose, catalytic studies were performed. Catalytic activity was studied by the measurement of oxygenate conversion

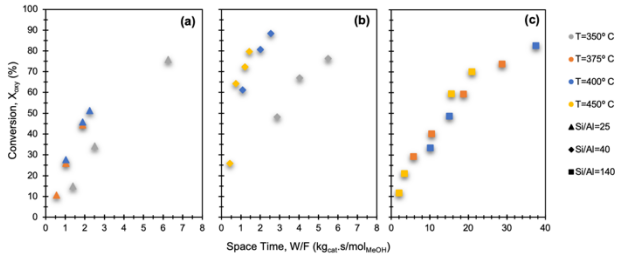

Figure 9 – Oxygenate conversion of MTO as function of space-time of H-ZSM-5 Si/Al of (a) 25, (b) 40, and (c) 140, at different temperatures. Conditions: T=[350, 450]° C, P_{MeOH}=0.4 bar, W/F=[0.5, 40.0] $kg_{cat}.s/mol_{MeOH}$.

with space-time of the selected data from the data assessment procedure (Figure 9). In this analysis, an approximation of a first-order kinetics (concerning oxygenates and olefins formation). The apparent activation energy was determined. Table 2 summarizes these results.

Data presents an increase in oxygenate conversion with increasing space-time and increasing temperature. Although less than optimal, for this analysis points outside the 20-80% oxygenate conversion window were considered for catalytic activity determination in order to not obtain linear regression with only 2 data points (as it would be the case for S25 and S40). As expected, catalytic activity was observed to decrease from S40 to S140 due to the increase in acid site density.

Table 2 – Kinetic parameters calculated for H-ZSM-5 Si/Al of 25, 40, and 140 (T=[350, 450]° C, P_{MeOH}=0.4 bar).

	Catalytic Activity, $k_{app} \cdot P^0_{MeOH}$ ($mol/kg_{cat}.s$)				$E_{A,app}$ (kJ/mol)
	350° C	375° C	400° C	450° C	
S25	0.21	0.30	0.32	--	45
S40	0.26	--	0.89	1.11	85
S140	--	0.05	0.05	0.06	14

Although good linear regressions from the logarithmic plots of conversion were found in the calculations (R^2>98%), S25 presented lower catalytic activity than S40. At 400° C and comparable space-times (2.3 and 2.0 $kg_{cat}.s/mol_{MeOH}$, respectively), a difference in conversion is observed from 51% to 81% for S25 and S40. Both data obtained at 350° C and 375° C display similar deactivation in S25. From the obstacles faced during the catalytic tests, this result was foreseen since all data acquired for this catalyst already displayed indications of deactivation. However, it is reasonable that activation energy did not suffer a deviation if a similar degree of deactivation (i.e., a similar shift in space-time) is hypothesized. Since deactivation is unmistakable present in S25, the validation of intrinsic kinetics cannot be guaranteed.

In the case of S140, at 450° C and similar space-times (1.4 and 2.1 $kg_{cat}.s/mol_{MeOH}$, respectively), the more acidic catalyst presents a steady-state conversion of 80% compared to 12%. This portrays the 20 times lower catalytic activity of this catalyst at this temperature.

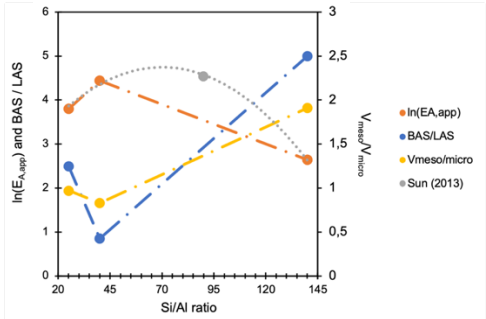

Figure 10 – Plot of ln($E_{A,app}$) of S25, S40, S140 obtained experimentally and of Si/Al 90 from Sun [21]; ratio of mesoporous and microporous volume and plot of the ratio of strong BAS/LAS, as a functions of catalyst Si/Al ratio.

Apparent activation energies of 45, 85, and 14 (kJ/mol were calculated for the three catalysts. Sun (2013) reported in his work an apparent activation energy of 93 kJ/mol for H-

ZSM-5 Si/Al of 90 [21]. In Figure 10 are plotted the results for these apparent activation energies, strong BAS/LAS ratios and mesoporous/microporous volume ratios as functions of H-ZSM-5 Si/Al, and a clear polynomial pattern is evident from this representation denoting the dependency of catalytic activity on catalyst textural properties and acidity. Moreover, from Figure 9 is observed a modest degree of overlapping of data between 375º C and 400º C, denoting a possible regime transition in these temperatures. These observations are further explored in the product distribution analysis section.

Product Distribution MTO product distribution consists essentially of unreacted methanol, DME, and C_2-C_4 olefins, C_{5+} aliphatic and aromatic hydrocarbon products. In this work, a thorough study of the effect of conversion on selectivity across the different catalysts revealed that selectivity does not suffer variations over 5% (on average) within the 20-80% oxygenate conversion range. This observation had also been concluded by the studies of Sun (2013) [21]. Ethylene/isobutane (E/Isob) and alkane/alkene (A/A) ratios were also used for the study of mechanistic phenomena. These ratios have been used as descriptors of the contribution of the aromatic/olefin cycles and the extent of hydrogen transfer reactions (responsible for the formation of alkanes and cyclization reactions), respectively, by several authors [20, 51]. The combined analysis of product distribution, E/Isob and A/A ratios uncovered the promotion of the aromatic cycle with increasing oxygenate conversion, which reaches a maximum at approximately 60% conversion. Here, C_{2-3} and C_{6+} hydrocarbons present a maximum of selectivity, whereas C_{4-5} and aromatics present a minimum. From thereon, the alkene cycle's predominance starts to increase. Catalyst acidity (i.e., increasing acid site density) appears to shift this inflexion point to lower conversions.

In Figure 11 are depicted the results of the catalytic tests performed between 350º and 450º C. As studied by Ilias et al. (2013), Sun (2013), Losch (2016) and many others, with increasing temperature it is observed the promotion of the alkene cycle in MTO, together with the promotion of

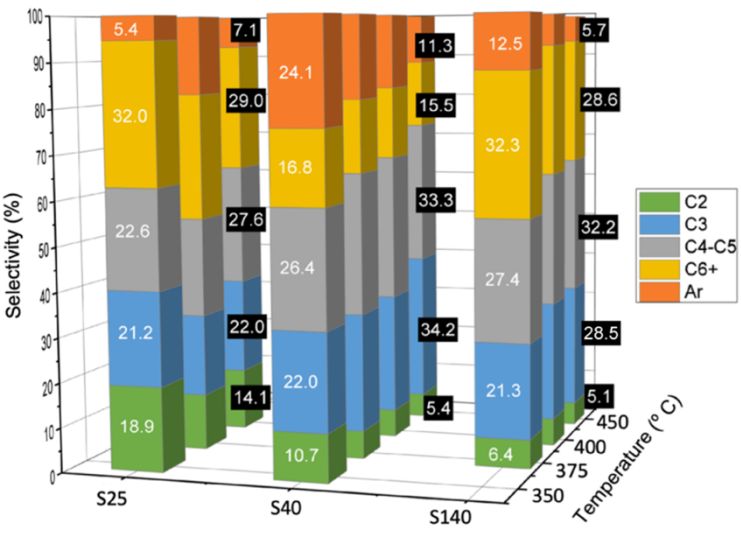

Figure 11 – Effect of H-ZSM-5 Si/Al ratio and temperature on the averaged product distribution of MTO, within the range of oxygenate conversion of 20-80% and P_{MeOH}=0.4 bar.

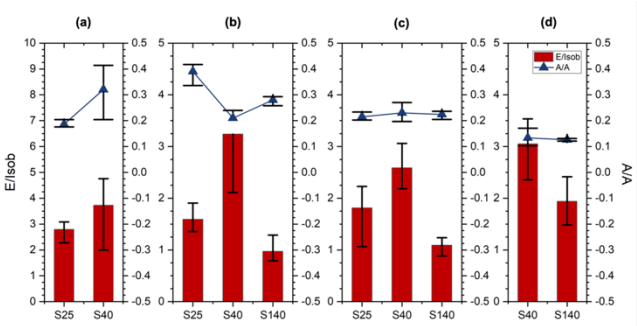

Figure 12 – Effect of H-ZSM-5 Si/Al ratio on the averaged ratio of E/Isob and A/A on MTO at (a) 350º C, (b) 375º C, (c) 400º C, and (d) 350º C, within the range of oxygenate conversion of 20-80% and P_{MeOH}=0.4 bar.

propylene yield [20, 21, 52]. In the present study, the best propylene yield maximization was achieved by S40, with 34% selectivity at 450º C (propylene/ethylene ratio of 5.3).

Furthermore, the effect of temperatures was portrayed by an increase in the alkene cycle propagation that changed at 375º C/400º C, from where the aromatic cycle resumed its prevailing influence (Figure 12). At lower temperatures, the analysis of the product distribution indicates an increase in lower olefin methylation and cracking reactions at a faster rate than oligomerization and higher olefin methylation reactions. Above 375º C, the decrease in aromatic products whilst maintaining C_2 yielding corroborates one of Pessanha's hypotheses: the rate at which aromatic methylation and dealkylation reactions occur increases substantially with increasing temperature [27]. This formulation is reasonable since these reactions would mainly form poly-MB intermediates, which would have high diffusion limitations and result in the observed higher deactivation rate with increasing temperature.

This observation is directly connected to the previous observations of catalytic activity. With Brønsted acid site density reduced to strong acidity with an accentuated decrease in BAS/LAS ratio), the results suggest that Lewis acidity is linked to the propagation of the aromatic cycle. Furthermore, the previous analysis on selectivity indicates that ethylene is primarily methylated over propylene.

Throughout the comparison of the three catalysts, S40 stands out with the increased aromatic selectivity (Figure 13). The greatest change is observed between S25 and S40 at 350º C (iso-temperature), with aromatic selectivity observing an increase in 380%. Although comparing at a higher temperature, when comparing S140 to S40 (450º C) comparable selectivities are found for C_2 and C_{4-5}. The greatest change noted is the increase in 81% and decrease in 46% of C_{6+} and aromatic yields, a pattern common to all temperatures, which remarks the influence of the aromatic cycle in S40 (Figure 12), with the decline of higher olefin methylation reaction rates.

S140, in contrast with S25, depicts a higher prevalence of the alkene cycle with E/Isob ratios 40% lower for both 375º C and 400º C. The key product distribution differences between these two catalysts reside

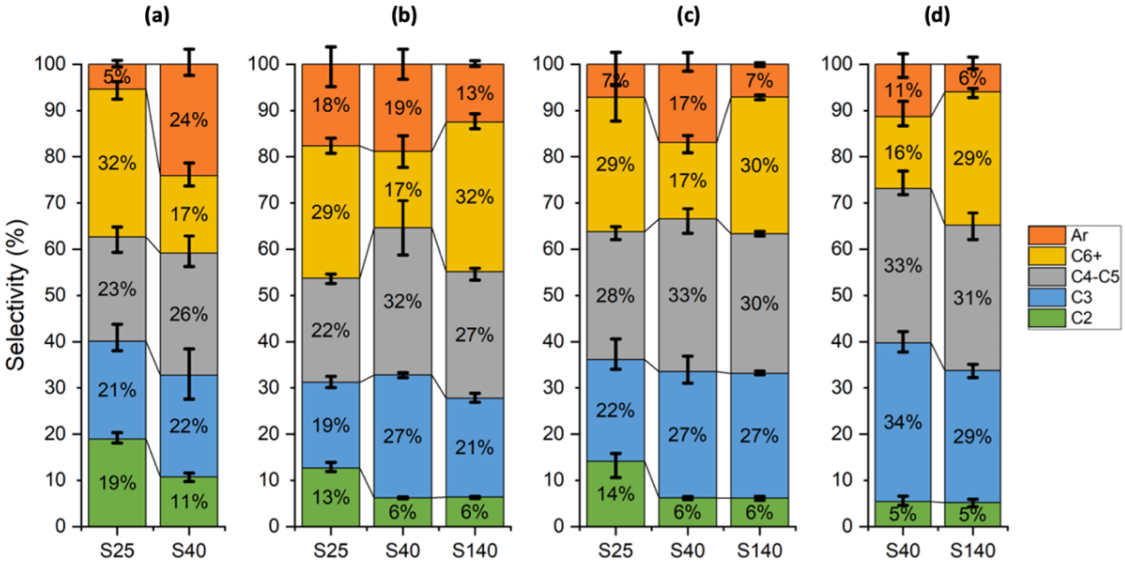

Figure 13 – Effect of H-ZSM-5 Si/Al ratio on the averaged product distribution of MTO at (a) 350º C, (b) 375º C, (c) 400º C, and (d) 350º C, within the range of oxygenate conversion of 20-80% and P_{MeOH}=0.4 bar.

in ethylene and aromatic yields, which present 28% and 54% lower selectivities for S140. This is followed by a small increase in propylene yield (11%) at 375º C, and an increase of 23% and 10% for C_{4-5} and C_{6+} hydrocarbons. Therefore, S25 appears to follow faster aromatic formation reactions (cyclization dealkylations, etc.) and S140 higher rates of alkene methylation reaction, resulting in increased ethylene and lower aromatic species for S25.

4. *Conclusion and Prospects*

These results implicate that lower BAS_{strong}/LAS_{total} ratios appear to be directly linked with the propagation of the aromatic cycle. More specifically, Brønsted acid sites can be associated with the effect of temperature until 375º C and 400º C. The effect of acidity is expressed by the increased promotion of the aromatic cycle with increasing temperature. Equivalent formulations are found scattered in the literature, namely, by the works of Huang et al. (2019) and Feng et al. (2020) [22, 23]. The first authors corroborated the promotion of the aromatic up an inflexion point, located at precisely between Si/Al of 50 and 200. From the observations in this work, this range can be narrowed down to an inflexion point possibly located between Si/Al of 100 and 140 (also considering Sun's work [21]). Feng and their colleagues ascribed the better propylene performance to lower strong acid site density (translated in lower BAS_{strong}/LAS_{total} ratios).

The defective sites encountered in S140 and S25 have been negatively associated to coke capacity and coke mobility [53]. Furthermore, these defects (with little to no acidity) could be implicated with the lower relative LAS when comparing S25 to S40. These premises are sustained when, in addition to the presence of higher strong BAS (where coke is preferentially deposited), S25 presents a higher deactivation rate than S40 whilst presenting similar catalytic activity. In support of the works of Djoko and Hartanto et al., structural defects manifest stabilization of Brønsted acidity from the preservation of BAS/LAS ratio with increasing temperature in S25 and S140 [38, 48].

The higher relative mesopore volume and external area in S140 are responsible for the much lower deactivation rate of this catalyst. The textural properties, together with the low acid site density, results in higher distances between active centres (isolated BAS), which per the works of Yarulina et al. (2018), is translated into improved propylene yield and improved catalyst lifetime [14].

Since S25 and S40 present similar LAS densities, whereas S25 and S40 display higher relative strong acidity (higher strong/weak acidity ratio), it results in the hypothesis that strong BAS is linked to the propagation of the alkene homologation cycle (primarily, alkene methylation and cracking reactions). Moreover, LAS present as being the preferential centres to catalyse dealkylation and cyclization reactions by the stabilization of intermediate polyMB species, providing higher propylene and aromatic content, as observed in S40. Therefore, LAS should also be responsible for the higher apparent activation energy observed in this catalyst.

Several studies that focused on the maximization of aromatic yield (methanol-to-aromatics process) support these conclusions, providing that Lewis acid sites are favourable to the aromatization of olefins from which MB are formed [54-58].

The present work allowed to deepen the understanding of the effect of H-ZSM-5 acidity, with validation from scattered knowledge found in the literature. Despite S40 presenting a better propylene yield maximization, S140 also displayed a good olefin yielding whilst maintaining a much higher catalyst lifetime. For industrial applications, S140 emerges with a much higher interest. Furthermore, the claims presented in this work can be found scattered in several studies in the literature.

Nonetheless, it is not entirely conclusive the pathway followed by either LAS or BAS, whether these acid sites are mechanism selective or not. However, it is clear how MTO is a catalysed reaction in two acid site types. Future catalytic studies, taking heed to intrinsic kinetic data acquisition, should focus on improving the understanding of the effect of acidity in order to build a reliable kinetic model.

5. References

[1] Boffey, D. (2020, Oct. 8). EU parliament votes for 60% greenhouse gas emissions cut by 2030. The Guardian.

[2] Rodgers, B. L. (2018, Dec. 17). Climate change: The massive CO_2 emitter you may not know about. BBC News.

[3] Cembureau (2020) Cementing: The European Green Deal.

[4] Polymer Solutions News Team. (2016, Aug. 16). Polyolefins are Everywhere! Polymer Solutions Incorporated.

[5] National Academies of Sciences, Engineering, and Medicine 2016. The Changing Landscape of Hydrocarbon Feedstocks for Chemical Production: Implications for Catalysis: Proceedings of a Workshop. Washington, DC: The National Academies Press. doi: 10.17226/23555.

[6] GlobalData. (2021, Jan. 5). China to lead global propylene capacity additions by 2030.

[7] GlobalData. (2020, December). Global Ethylene Capacity and Capital Expenditure Outlook to 2030 - Asia Leads Globally in Terms of Ethylene Capacity Additions.

[8] Eramo, M. (2019, March 20). Global basic chemicals outlook. IHS Markit.

[9] How to Make Propylene and Ethylene at the Lowest Cash Cost of Production? (2019, Sept. 17). How To Find The Money.

[10] Brian M. Harney (1975) Methanol from Coal-A Step Toward Energy Self-Sufficiency, Energy Sources, 2:3, 233-249, doi: 10.1080/00908317508945951

[11] Khalafalla, S. S., Zahid, U., Abdul Jameel, A. G., Ahmed, U., Alenazey, F. S., & Lee, C.-J. (2020). Conceptual Design Development of Coal-to-Methanol Process with Carbon Capture and Utilization. Energies, 13(23), 6421. doi:10.3390/en13236421

[12] Sherrard, A. (2020, October 25). Belgian stakeholders launch North-C-Methanol project. Bioenergy International.

[13] Stöcker, M. (1999). Methanol-to-hydrocarbons: catalytic materials and their behavior. Microporous and Mesoporous Materials, 29(1-2), 3–48. doi:10.1016/s1387-1811(98)00319-9

[14] Yarulina, I., Chowdhury, A. D., Meirer, F., Weckhuysen, B. M., & Gascon, J. (2018). Recent trends and fundamental insights in the methanol-to-hydrocarbons process. Nature Catalysis, 1(6), 398–411. doi:10.1038/s41929-018-0078-5

[15] Olsbye, U., Svelle, S., Bjørgen, M., Beato, P., Janssens, T. V. W., Joensen, F., Bordiga, S., & Lillerud, K. P. (2012). Conversion of Methanol to Hydrocarbons: How Zeolite Cavity and Pore Size Controls Product Selectivity. Angewandte Chemie International Edition, 51(24), 5810–5831. doi:10.1002/anie.201103657

[16] Xu, S., Zhi, Y., Han, J., Zhang, W., Wu, X., Sun, T., … Liu, Z. (2017). Advances in Catalysis for Methanol-to-Olefins Conversion. Advances in Catalysis, 37–122. doi:10.1016/bs.acat.2017.10.002

[17] Svelle, S., Joensen, F., Nerlov, J., Olsbye, U., Lillerud, K.-P., Kolboe, S., & Bjørgen, M. (2006). Conversion of Methanol into Hydrocarbons over Zeolite H-ZSM-5: Ethene Formation Is Mechanistically Separated from the Formation of Higher Alkenes. Journal of the American Chemical Society, 128(46), 14770–1477. doi:10.1021/ja065810a

[18] Dahl, I. M., & Kolboe, S. (1994). On the Reaction Mechanism for Hydrocarbon Formation from Methanol over SAPO-34. Journal of Catalysis, 149(2), 458–464. doi:10.1006/jcat.1994.1312

[19] Yarulina, I., Chowdhury, A. D., Meirer, F., Weckhuysen, B. M., & Gascon, J. (2018). Recent trends and fundamental insights in the methanol-to-hydrocarbons process. Nature Catalysis, 1(6), 398–411. doi:10.1038/s41929-018-0078-5

[20] Ilias, S., Khare, R., Malek, A., & Bhan, A. (2013). A descriptor for the relative propagation of the aromatic- and olefin-based cycles in methanol-to-hydrocarbons conversion on H-ZSM-5. Journal of Catalysis, 303, 135–140. doi:10.1016/j.jcat.2013.03.021

[21] Xianyong Sun. (2013). Catalytic Conversion of Methanol to Olefins over HZSM-5 Catalysts. Thesis to achieve Complete imprint of the from the Faculty of Chemistry at the Technical University of Munich (Germany) to obtain the academic degree of Doctor of Natural Sciences (Dr. rer. Nat.) (2013).

[22] Huang, H., Zhu, H., Zhang, S., Zhang, Q., & Li, C. (2019). Effect of silicon to aluminum ratio on the selectivity to propene in methanol conversion over H-ZSM-5 zeolites. Journal of Fuel Chemistry and Technology, 47(1), 74–82. doi:10.1016/s1872-5813(19)30005-2

[23] Feng, R., Yan, X., Hu, X., Wu, J., & Yan, Z. (2020). Direct synthesis of b-axis oriented H-form ZSM-5 zeolites with an enhanced performance in the methanol to propylene reaction. Microporous and Mesoporous Materials, 302, 110246. doi:10.1016/j.micromeso.2020.110246

[24] Liang, T., Chen, J., Qin, Z., Li, J., Wang, P., Wang, S., Wang, G., Dong, M., Fan, W., & Wang, J. (2016). Conversion of Methanol to Olefins over H-ZSM-5 Zeolite: Reaction Pathway Is Related to the Framework Aluminum Siting. ACS Catalysis, 6(11), 7311–7325. doi:10.1021/acscatal.6b01771

[25] Pit Losch. Synthesis and characterisation of zeolites, their application in catalysis and subsequent rationalisation : methanol-to-olefins (MTO) process with designed ZSM-5 zeolites. Catalysis. Université de Strasbourg, 2016. English.

[26] Standl, S., & Hinrichsen, O. (2018). Kinetic Modeling of Catalytic Olefin Cracking and Methanol-to-Olefins (MTO) over Zeolites: A Review. Catalysts, 8(12), 626. doi:10.3390/catal8120626

[27] Bernardo Pessanha. (2019). A Steady State Study: Effect of Zeolite and Operating Conditions on Methanol-to-Olefins. Thesis to obtain the Master of Science Degree in Chemical Engineering. Instituto Superior Técnico (IST, UL), Portugal.

[28] Phung, Thanh Khoa; Busca, Guido (2014). On the Lewis acidity of protonic zeolites. Applied Catalysis A: General, (2014). doi:10.1016/j.apcata.2014.11.031

[29] "ZSM-5." ACS Material Store, ACS Material

[30] Peng, P., Wang, Y., Rood, M (et al.) Zhang, Z., & Gao, X. (2015). Effects of dissolution alkalinity and self-assembly on ZSM-5-based micro-/mesoporous composites: a study of the relationship between porosity, acidity, and catalytic performance. CrystEngComm, 17(20), 3820–3828. doi: 10.1039/c5ce00384a

[31] Sing, K. S. W., & Williams, R. T. (2004). Physisorption Hysteresis Loops and the Characterization of Nanoporous Materials. Adsorption Science & Technology, 22(10), 773–782. doi:10.1260/0263617053499032

[32] Weissenberger, T., Machoke, A. G. F., Bauer, J., Dotzel, R., Casci, J. L., Hartmann, M., & Schwieger, W. (2020). Hierarchical ZSM-5 Catalysts: The Effect of Different Intracrystalline Pore Dimensions on Catalyst Deactivation Behaviour in the MTO Reaction. ChemCatChem, 12(9), 2461–2468. doi:10.1002/cctc.201902362

[33] Reis Bernardes, F., Jakeline Cunha Rezende, M., de Oliveira Rodrigues, V., Sandra Veiga Nascimento, R., & Pereira da Silva Ribeiro, S. (2019). Synthesis and Application of H-ZSM-5 Zeolites with Different Levels of Acidity as Synergistic Agents in Flame Retardant Polymeric Materials. Polymers, 11(12), 2110. doi:10.3390/polym11122110

[34] Hu, S., Shan, J., Zhang, Q., Wang, Y., Liu, Y., Gong, Y., Wu, Z., & Dou, T. (2012). Selective formation of propylene from methanol over high-silica nanosheets of MFI zeolite. Applied Catalysis A: General, 445–446, 215–220. doi:10.1016/j.apcata.2012.08.032

[35] Gabrienko, Anton A.; Danilova, Irina G.; Arzumanov, Sergei S.; Pirutko, Larisa V.; Freude, Dieter; Stepanov, Alexander G. (2018). Direct Measurement of Zeolite Brønsted Acidity by FTIR Spectroscopy: Solid-State ^{1}H MAS NMR Approach for Reliable Determination of the Integrated Molar Absorption Coefficients. J. Phys. Chem. C 2018, 122, 44, 25386–25395. doi:10.1021/acs.jpcc.8b07429

[36] Newland, Stephanie H.; Sinkler, Wharton; Mezza, Thomas; Bare, Simon R.; Raja, Robert (2016). Influence of dopant substitution mechanism on catalytic properties within hierarchical architectures. Proceedings of the Royal Society A: Mathematical, Physical and Engineering Science, 472(2191), 20160095–.doi:10.1098/rspa.2016.0095

[37] Fang Jin; Yongdan Li (2009). A FTIR and TPD examination of the distributive properties of acid sites on ZSM-5 zeolite with pyridine as a probe molecule. Catalysis Today 145(1-2), 101–107. doi:10.1016/j.cattod.2008.06.007

[38] Anton A. Gabrienko; Irina G. Danilova; Sergei S. Arzumanov; Alexander V. Toktarev; Dieter Freude; Alexander G. Stepanov (2010). Strong acidity of silanol groups of zeolite beta: Evidence from the studies by IR spectroscopy of adsorbed CO and ^{1}H MAS NMR. Microporous and Mesoporous Materials 131, 210–216. doi:10.1016/j.micromeso.2009.12.025

[39] Luz Rodríguez-González; Florian Hermes; Marko Bertmer; Enrique Rodríguez-Castellón; Antonio Jiménez-López; Ulrich Simon (2007). The acid properties of H-ZSM-5 as studied by NH3-TPD and ^{27}Al-MAS-NMR spectroscopy. , 328(2), 174–182.doi:10.1016/j.apcata.2007.06.003

[40] Epelde, Eva; Santos, José I.; Florian, Pierre; Aguayo, Andrés T.; Gayubo, Ana G.; Bilbao, Javier; Castaño, Pedro (2015). Controlling coke deactivation and crackig selectivity of MFI zeolite by H_3PO_4 or KOH modification. Applied Catalysis A: General 505. doi:10.1016/j.apcata.2015.07.022

[41] Petr Sazama; Blanka Wichterlova; Jiri Dedecek; Zdenka Tvaruzkova; Zuzana Musilova; Luisa Palumbo; Stepan Sklenak; Olga Gonsiorova (2011). FTIR and ^{27}Al MAS NMR analysis of the effect of framework Al- and Si-defects in micro- and micro-mesoporous H-ZSM-5 on conversion of methanol to hydrocarbons. , 143(1), 87–96. doi:10.1016/j.micromeso.2011.02.013

[42] S. Bordiga; C. Lamberti; F. Bonino; A. Travert; F. Thibault-starzyk (2015). Probing zeolites by vibrational spectroscopies. Chem. Soc. Rev., 2015,44, 7262-7341. doi:10.1039/C5CS00396B

[43] Belskaya, Olga B.; Danilova, Irina G.; Kazakov, Maxim O.; Mironenko, Roman M.; Lavrenov, Alexander V.; Likholobov, Vladimir A. (2013). ChemInform Abstract: FTIR Spectroscopy of Adsorbed Probe Molecules for Analyzing the Surface Properties of Supported Pt (Pd) Catalysts. ChemInform, 44(51), doi:10.1002/chin.201351237

[44] Zambare, Abhay Suresh; Ou, John; Hill Wong, David Shan; Yao, Ching-Wen; Jang, Shi-Shang (2019). Controlling the product selectivity in the conversion of methanol to the feedstock for phenol production. RSC Advances, 9(41), 23864–23875. doi:10.1039/c9ra03723c

[45] Barzetti, Tommy; Selli, Elena; Moscotti, Daniele; Forni, Lucio (1996). Pyridine and ammonia as probes for FTIR analysis of solid acid catalysts. Journal of the Chemical Society, Faraday Transactions, 92(8), 1401. doi:10.1039/FT9969201401

[46] C.A. Emeis (1993). Determination of Integrated Molar Extinction Coefficients for Infrared Absorption Bands of Pyridine Adsorbed on Solid Acid Catalysts. , 141(2), 347–354. doi:10.1006/jcat.1993.1145

[47] Puértolas, B., Veses, A., Callén, M. S., Mitchell, S., García, T., & Pérez-Ramírez, J. (2015). Porosity-Acidity Interplay in Hierarchical ZSM-5 Zeolites for Pyrolysis Oil Valorization to Aromatics. ChemSusChem, 8(19), 3283–3293. doi:10.1002/cssc.201500685

[48] Hartanto, Djoko; Sin Yuan, Lai; Mutia Sari, Sestriana; Sugiarso, Djarot; Kris Murwarni, Irmina; Ersam, Taslim; Prasetyoko, Didik; Nur, Hadi (2016). The Use Of The Combination Of Ftir, Pyridine Adsorption, ^{27}Al and ^{29}Si MAS NMR To Determine The Brönsted And Lewis Acidic Sites. Jurnal Teknologi, 78(6). doi:10.11113/jt.v78.8821

[49] Hazrati, Hossein. (2018). Selective production of light olefins from methanol over desilicated highly siliceous ZSM-5 nanocatalysts. Polyolefins Journal. 5. doi:10.22063/poj.2017.1501

[50] Bailleul, S., Yarulina, I., Hoffman, A. E. J., Dokania, A., Abou-Hamad, E., Chowdhury, A. D., Pieters, G., Hajek, J., De Wispelaere, K., Waroquier, M., Gascon, J., & Van Speybroeck, V. (2019). A Supramolecular View on the Cooperative Role of Brønsted and Lewis Acid Sites in Zeolites for Methanol Conversion. Journal of the American Chemical Society, 141(37), 14823–14842. doi:10.1021/jacs.9b07484

[51] Ibáñez, M.; Pérez-Uriarte, P.; Sánchez-Contador, M.; Cordero-Lanzac, T.; Aguayo, A.T.; Bilbao, J.; Castaño, P. (2017). Nature and Location of Carbonaceous Species in a Composite HZSM-5 Zeolite Catalyst during the Conversion of Dimethyl Ether into Light Olefins. Catalysts 2017, 7, 254. doi: 10.3390/catal7090254

[52] Pit Losch. Synthesis and characterisation of zeolites, their application in catalysis and subsequent rationalisation : methanol-to-olefins (MTO) process with designed ZSM-5 zeolites. Catalysis. Université de Strasbourg, 2016. English. NNT : 2016STRAF035 . tel-01531844

[53] Meng, Xiaojing; Zhang, Minxiu; Chen, Chunlin; Li, Chunyi; Xiong, Wei; Li, Min (2018). Insights into the role of silanols in methanol to propene reaction over silicalite-2 zeolite through post-treatments. Applied Catalysis A: General, 558(), 122–130. doi:10.1016/j.apcata.2018.04.001

[54] Li, T., Shoinkhorova, T., Gascon, J., & Ruiz-Martínez, J. (2021). Aromatics Production via Methanol-Mediated Transformation Routes. ACS Catalysis, 11(13), 7780–7819.doi:10.1021/acscatal.1c01422

[55] Lin, S., Zhi, Y., Chen, W., Li, H., Zhang, W., Lou, C., … Liu, Z. (2021). Molecular Routes of Dynamic Autocatalysis for Methanol-to-Hydrocarbons Reaction. Journal of the American Chemical Society, 143(31), 12038–12052.doi:10.1021/jacs.1c03475

[56] Róbert Barthos; Tamás Bánsági; Tímea Süli Zakar; Frigyes Solymosi (2007). Aromatization of methanol and methylation of benzene over Mo2C/ZSM-5 catalysts. Journal of Catalysis 247 (2007) 368–378. doi:10.1016/j.jcat.2007.02.017

[57] Lezcano Castillo, Gontzal. (2018). Kinetic modelling of the dimethyl ether to olefins reaction over a HZSM-5 based catalyst. Thesis to obtain the Bachelor's degree in Chemical Engineering. Universidad del País Vasco.

[58] VanSpeybroeck, Veronique; De Wispelaere, Kristof; Van der Mynsbrugge, Jeroen; Vandichel, Matthias; Hemelsoet, Karen; Waroquier, Michel (2014). First principle chemical kinetics in zeolites: the methanol-to-olefin process as a case study. Chem. Soc. Rev., 43(21), 7326–7357. doi:10.1039/C4CS00146J